Energy-resolved coincidence counting using an FPGA for nuclear lifetime experiments

Mario Vretenar, Nataša Erceg, and Marin Karuza

Citation: American Journal of Physics **87**, 997 (2019); doi: 10.1119/1.5122744
View online: https://doi.org/10.1119/1.5122744
View Table of Contents: https://aapt.scitation.org/toc/ajp/87/12
Published by the American Association of Physics Teachers

APPARATUS AND DEMONSTRATION NOTES

The downloaded PDF for any Note in this section contains all the Notes in this section.

John Essick, *Editor*
Department of Physics, Reed College, Portland, OR 97202

Articles in this section deal with new ideas and techniques for instructional laboratory exercises, for demonstrations and for equipment that can be used in either. Although these facets of instruction also appear in regular articles, this section is for papers that primarily focus on equipment, materials and how they are used in instruction.

Manuscripts should be submitted using the web-based system that can be accessed via the *American Journal of Physics* home page, http://web.mit.edu/rhprice/www, and will be forwarded to the ADN editor for consideration.

Energy-resolved coincidence counting using an FPGA for nuclear lifetime experiments

Mario Vretenar and Nataša Erceg
Department of Physics, University of Rijeka, Rijeka 51000, Croatia

Marin Karuza[a)]
Department of Physics, University of Rijeka, Rijeka 51000, Croatia; CMNST and Center of Excellence for Advanced Materials and Sensing Devices, Photonics and Quantum Optics group, University of Rijeka, Rijeka 51000, Croatia; and INFN Sezione di Trieste, Trieste 34127, Italy

(Received 3 January 2018; accepted 29 July 2019)

With the increasing availability of single-board computers equipped with fast analog-to-digital converters based on field-programmable gate arrays (FPGA), researchers and educators gain access to relatively inexpensive hardware that can be programmed for advanced coincidence counting. We demonstrate this capability by developing software for a dual-channel open-source data acquisition platform, enabling it to perform energy- and time-resolved coincidence counting and testing our system using an ^{241}Am source. Measuring the coincidence between alpha and gamma radiation allowed us to determine the half-life of the ^{237}Np excited state. The obtained value of 67.7 ± 0.1 ns is compatible with the value cited in the literature. Furthermore, the use of digital signal processing enabled us to sort time-resolved counts by alpha and gamma energy, which resulted in additional information on the decay scheme. Correlation heatmaps between the two spectra were plotted and used to verify the decay scheme. The half-lives of the other features visible in the gamma spectrum were determined as well.
https://doi.org/10.1119/1.5122744

I. INTRODUCTION

Coincidence counting is a powerful technique with many applications, one of which is providing information about nuclear states. Unfortunately, such measurements often require dedicated hardware that is normally not available to the educators at the high school or even university level. In this article, we focus on an $\alpha - \gamma$ coincidence measurement, although the software we develop may be adapted for other kinds of events as well. We choose to study ^{241}Am, following a number of decades-old articles[1,2] and applying modern electronics and digital signal processing techniques[3–5] in order to demonstrate that one may extract additional information from coincidence counting measurements by thorough post-processing. As the above-mentioned articles demonstrate, it is possible to determine the half-life of a nuclear state by fitting an exponential function onto the delay graph. We show that by sorting events not just by delay, but by alpha and gamma energies as well, it is possible to simultaneously inspect multiple transitions and get even more insight into the nature of unresolved peaks.

Alpha decay can be explained using quantum mechanical concepts taught at the undergraduate level. Thus this process is understandable to physics students and, at the same time, gives insight into nuclear structure and decay schemes. The measurements of nuclear lifetimes historically included the use of dedicated equipment, which could be found only in research laboratories. Besides alpha and gamma radiation detectors, this research instrumentation also included time-to-voltage converters and multichannel analyzers. In such setups, the need to convert time to voltage is a step that can mislead a student, but with advent of fast analog-to-digital converters (ADC) and field-programmable gate arrays (FPGA) this step can be skipped and the measurements become much more accessible in an undergraduate physics laboratory. Here, we describe a simple low-cost experiment using the Red Pitaya single-board computer (SBC). This approach, where the intermediate step of converting time to

voltage is omitted, is clearer to the average student since times are directly measured. Although alpha decay is not directly studied with this experiment, we will give a short overview of the process.

A. The decay scheme

Alpha decay is a (surprisingly) pure quantum mechanical phenomenon in which a particle tunnels through a barrier equal to the sum of the involved atom's nuclear and electromagnetic force potentials. The tunneling-particle is an alpha particle, consisting of two protons and two neutrons. Thus this process reduces the atom's atomic mass by four and its charge by two; the kinetic energy of the alpha particle is approximately 5 MeV. The recoil of the resulting nucleus can be approximated to zero since the mass ratio of the decay products is more than 50. The complete theoretical treatment of alpha decay has been done by Gamow and can be found in Ref. 6; for more material, see also Refs. 7 and 8. Furthermore, the resulting nucleus is often found in an excited nuclear state, which deexcites to the fundamental level by emission of gamma radiation or via other processes.

The decay scheme of ^{241}Am by alpha decay is shown in Fig. 1. As shown, when an ^{241}Am nucleus decays into ^{237}Np, several energies are possible for the emitted alpha particle, where each possibility is associated with an excited state of the ^{237}Np nucleus. Each excited states corresponds to the nucleons (protons and neutrons) occupying a higher-energy nuclear orbital in analogy with atomic excited states. Atoms with nuclei in excited states are called nuclear isomers and in most cases they deexcite on time scales of the order of ps. When the half-life is of the order of ns, or longer, then the nucleus is in the metastable state. The reason for a longer lifetime follows from conservation laws.[9] The most obvious example is the spin conservation law, where a large spin change makes the transition "forbidden." Other possibilities include shape[10] and K isomers. Isomer decays by proton or neutron emission or even fission along the alpha, beta, gamma decay, or internal conversion.[11] The process where the nucleus excess energy is used for the ionization of the atom where an electron from the inner orbitals is ejected is called internal conversion. In our case, about 84% of the decays result in the ^{237}Np nuclei being in the 59.5 keV excited-state level, where almost every subsequent deexcitation involves emission of 59.5 keV and 26.3 keV gamma photons. The half-life of 67.2 ns for this decay channel is considerably longer than the prompt emission lifetime, which is not surprising since it involves a large spin change. More details about ^{237}Np can be found in literature.[12] The most probable alpha decay emits an 5485.56 keV alpha particle. The other alpha lines, in particular, the one at 5442.8 keV, should also be visible in the alpha spectrum but won't be correlated with the most intense gamma lines in the gamma spectrum.

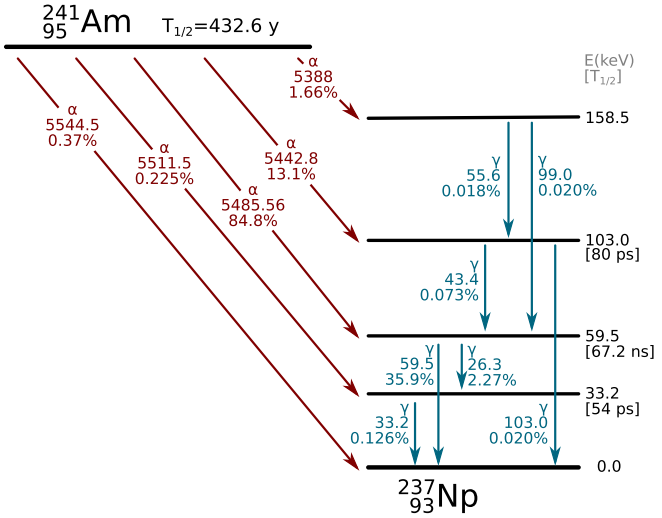

Fig. 1. The decay scheme of ^{241}Am. All energies are in keV. Only a fraction of excited nuclei decay by emission of a γ ray. The remaining decays take place by other processes. See text.

II. EXPERIMENTAL SETUP

A. Hardware

The heart of the experimental setup (Fig. 2) is the Red Pitaya v1.1 (Ref. 13) (in the following text, referred to as "RP"): an FPGA development board based on a Zynq 7010 SoC ("system on chip"), containing an ARM Dual Cortex A9 processor and a Xilinx FPGA. The board has two 125 MS/s 14-bit (RP version 1.1) ADCs internally connected to the FPGA and exposed through two SMA connectors, 512 MB of RAM, and a LAN port. These characteristics, combined with a relatively low cost (~$300) make it a suitable platform for developing a customized DAQ.

The radioactive ^{241}Am source (PHYWE 09090-11) internally wrapped up in ~2 μm of silver foil is placed inside a vacuum chamber (PHYWE 09103-00) kept at a constant pressure of 8 mbar during all measurements in order to reduce alpha-particle energy loss. The alpha detector (PHYWE 09100-00) is placed inside the vacuum chamber as well, while the gamma detector (PHYWE 09101-00) resided just outside, additionally shielded from background radiation by lead plates (Fig. 3). It was observed that the vacuum chamber glass walls slightly alter the measured gamma spectrum, however due to the large size of the gamma detector it had to be placed outside the chamber. The distances and angles between the source and the detectors were configured as to maximize the count rate without saturating the detectors.

The alpha detector is connected to the stock pre-amplifier (PHYWE 09100-10). The output of the pre-amplifier is connected to the channel A input of the RP, with an added parallel resistance of 10 kΩ in order to shorten the duration of the

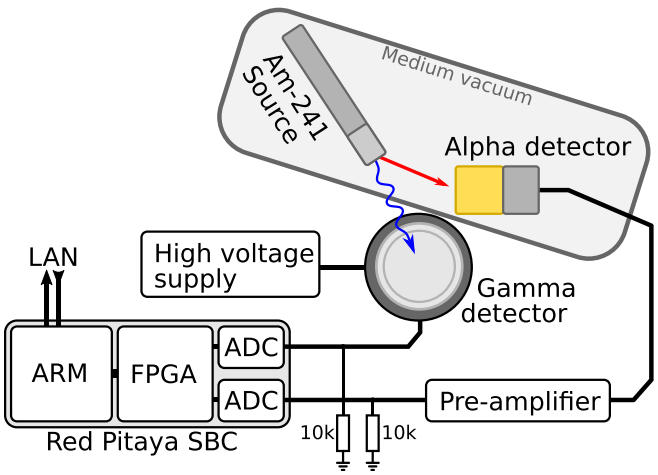

Fig. 2. The block diagram of the experimental setup.

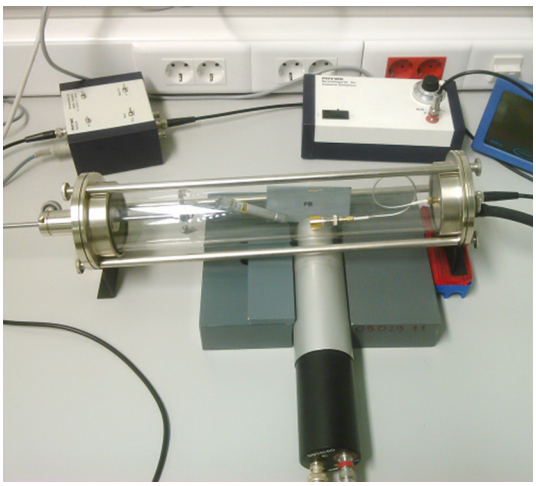

Fig. 3. Photograph showing the ^{241}Am source and alpha detector placed inside a vacuum chamber, with the gamma detector underneath.

pulses, replicating the input impedance of the single channel analyzer originally used with this detector. Similarly, the gamma detector is connected directly to the channel B input of the RP with an added resistance of 10 kΩ, for the same reason as the other channel. Although the spectra measured using the outputs provided by the stock pulse height analyzers (PHYWE 13725-93 (obsolete) and PHYWE 13727-99) were of a higher energy resolution due to the additional processing electronics (signal shaping), we were forced not to use them as they introduce jitter, which compromises the delay graph as can be seen in Fig. 4.

B. Software

The RP development board software is open source[14] and consists of an Linux operating system (Ubuntu), FPGA code, and an Nginx server providing access to multiple applications and development tools accessible via a web browser. The stock FPGA code provides a framework for using the board as an oscilloscope, a signal generator, spectrum analyzer, and a number of other devices. Coincidence counting can be implemented using the stock FPGA binaries with one of the channels as the trigger source. However, in this approach, the count rate will be low since the whole waveform following the trigger has to be transferred to the CPU and only one channel may be used as the trigger. In case the delays introduced by the detectors cause a portion of the events on the other channel to precede the trigger, that part of the event distribution will be lost. This may be countered by introducing hardware delays, which is impractical, or by writing dedicated coincidence counting FPGA code. Instead, we decided to rewrite parts of the FPGA code. We choose the RP firmware v0.96 FPGA code as the starting point and disabled the oscilloscope portion of the code to free enough logic to be able to add our own code. Our code is hosted on our Github repository[15] and consists of two parts: the Verilog HDL code that runs on the FPGA and the C++ code executed on the RP central processing unit in userspace.

Our FPGA code does the following: the analog input channels are monitored and once their value passes the specified trigger threshold, an event is initiated. A typical example of an (non-correlated) alpha and gamma event is shown in Fig. 5. Once the measured signal crosses the threshold (points 1 and 3 on the graph), the FPGA code notes the timestamp and records the extremum until the threshold is crossed again (points 2 and 4). Those two numbers, along with the channel id are then sent to the CPU via a shift register. Each channel has an independent and identical counter. For overlapping events (for example, if the point time arrangement were 1, 3, 4, 2 in Fig. 5), their order in the queue might not be chronological due to their duration. This is why they have to be sorted by timestamp on the CPU before further processing which is discussed below. The shift register ensures lossless continuous data transmission to the CPU. There are three configuration parameters per channel: trigger threshold, trigger edge, and minimum event duration (which can be configured to filter out unwanted short events caused by noise). The maximum signal value during the event represents the energy of the particle detected by the sensor. A possible improvement would be to integrate the peaks, which would further reduce the noise and may be implemented in future versions of the code. The FPGA code has to be compiled with the Xilinx Vivado tool (our repository also contains pre-compiled binaries). Our code does not support waveform acquisition so, in order to capture typical event waveforms, the stock FPGA binaries have to be used.

Our C++ code fetches the events from the shared queue and chronologically sorts them into a second queue. This process is done continuously: after each new event is added, the queue is sorted again, and once the oldest event is older than the newest one by a time larger than twice the

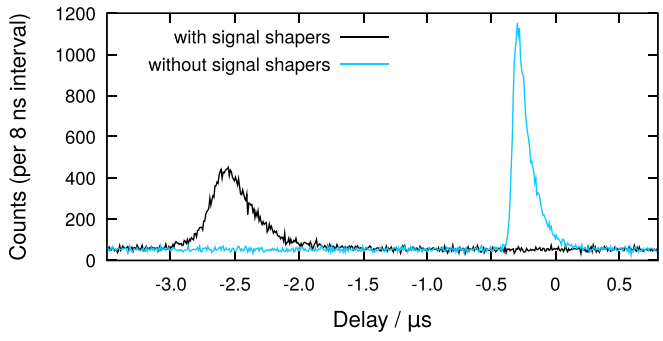

Fig. 4. Coincidence delay graph measured with and without external signal shapers on an ^{241}Am source, including all visible peaks. The delay represents the timestamp difference between the events; a negative value means that the event on channel B precedes the event on channel A. The shapers introduce additional delays and visibly distort the delay profile, significantly reducing the precision of the lifetime measurement. The acquisition time was 13 min.

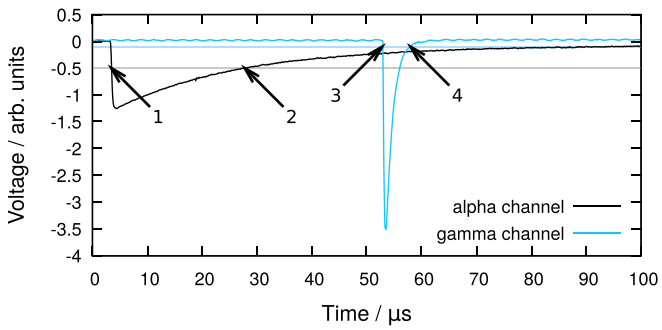

Fig. 5. A typical example of an (non-correlated) alpha and gamma event. A correlated event would have a much smaller delay between the peak starts due to the short ^{241}Am state lifetime (about 67 ns). The marks represent points at which the signals pass the pre-defined thresholds. Event triggers are indicated by marks 1 and 3, and ends by marks 2 and 4 for the alpha and the gamma channel, respectively.

coincidence window, it is removed. This time interval ensures that all events that may possibly overlap are being sorted by timestamp. The removed element is used as the trigger and is checked against all elements in the queue that are from the other channel: the timestamp difference and the event energies determine which integer of the 3D array used to store data should be incremented. These unsigned integers represent the number of counts within an 8 ns interval for the alpha and gamma energy step. The array is then saved on the RP SD card. The total time (coincidence window) and energy range which determine the binning may be specified via a configuration file. New counts can be appended to the previously acquired data, allowing the user to acquire data over multiple sessions. From this array one may plot a correlation heatmap,[16] single out certain transitions, and export their delay diagrams to determine half-life or export correlated spectra. It would also be possible to modify the user-space code to log events instead of filling bins, however this would rapidly take up space compared to binning, which has a constant file size independent of the number of recorded events.

The performance of the system predominately depends on the coincidence window and the count rate. For example, setting the coincidence window to 0.2 ms results in a maximum event frequency of about 20 kHz on both channels. Decreasing the window duration to 0.02 ms increases the maximum frequency to about 40 kHz on both channels. The performance seems to be limited by the sorting function that runs on the CPU; without it, the count rate would be on the order of 1 MHz, limited by the data transfer implementation on the FPGA.

III. RESULTS AND DISCUSSION

Data were acquired using the method explained above in a single continuous measurement taken over the course of 88 h. This dataset is used as a basis for all graphs and discussions presented in Secs. III A–III E.

A. Alpha spectrum

The measured alpha spectrum is shown on Fig. 6 (as the curve labeled "Measurement"). Although up to five peaks were expected from the decay scheme, the spectrum shows only a single wide apparent peak, corresponding to the most likely decay route. The poor alpha energy resolution is due to a malfunction of the pre-amplifier. Some additional information about the alpha spectrum may be deduced from the correlation data, which is discussed in Sec. III D.

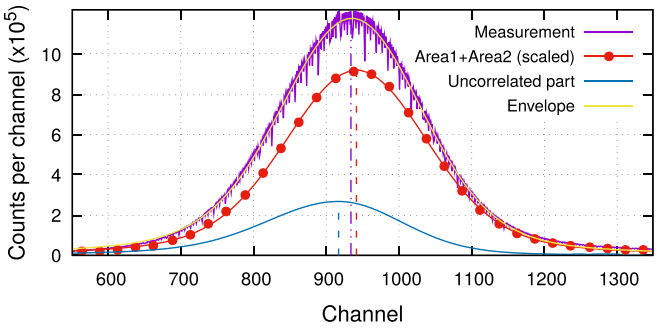

Fig. 6. Alpha spectrum with correlated data. The main peak is the total number of counts, the dots represent the correlated counts (each dot represents 25 α channels), and the lines are the curves fitted so that their sum matches the total number of counts.

B. Gamma spectrum

The duration of the measurement was dictated by the intent to resolve and correlate as many gamma peaks as possible. If one wishes to study only the peak at 59.5 keV, a much shorter measurement is sufficient, which is probably desirable for most undergraduate or graduate instructional lab experiments. However, longer measurements provide an insight into the lifetime of other states as well. First, the total gamma spectrum shown in Fig. 7 was evaluated, consisting of all detected gamma events. Two peaks are visible, one of which is the ^{241}Am gamma at 59.5 keV, while the other contains multiple smaller peaks, one of which is the ^{241}Am gamma at 26.3 keV. The spectrum was calibrated using the peak at 59.5 keV and the most intense peak in the lower-energy feature: the Iodine Kα escape line expected at 30.9 keV which is the energy difference between 59.5 keV gamma ray and Iodine Kα line at 28.61 keV. Iodine is found in the NaI scintillator used for gamma ray detection. A set of Voigt profiles with an asymmetric Lorentzian part and a Gaussian part linearly dependent on peak energy is fitted onto the spectrum. The Gnuplot's Voigt/Faddeeva[17] function approximation for the convolution of a Gaussian and Lorentzian was used, denoted as "Voigt" in the complete equation

$$N_n(h\nu) = A_n \cdot \begin{cases} \dfrac{\mathrm{Voigt}\left(\dfrac{\nu_n - \nu}{G_n \cdot \nu}, \dfrac{L_{\geq,n}}{G_n \cdot \nu}\right)}{\mathrm{Voigt}\left(0, \dfrac{L_{\geq,n}}{G_n \cdot \nu}\right)}, & \text{if } h\nu \geq h\nu_n \\ \dfrac{\mathrm{Voigt}\left(\dfrac{\nu_n - \nu}{G_n \cdot \nu}, \dfrac{L_{<,n}}{G_n \cdot \nu}\right)}{\mathrm{Voigt}\left(0, \dfrac{L_{<,n}}{G_n \cdot \nu}\right)}, & \text{otherwise,} \end{cases}$$

where N_n is the peak number of counts for the n-th peak, ν_n is the peak center frequency, G_n is the Gaussian parameter, and $L_{\geq,n}$ and $L_{<,n}$ are the Lorentzian parameters. The Voigt parameters (G_n, $L_{\geq,n}$, and $L_{<,n}$) are the same for the smaller

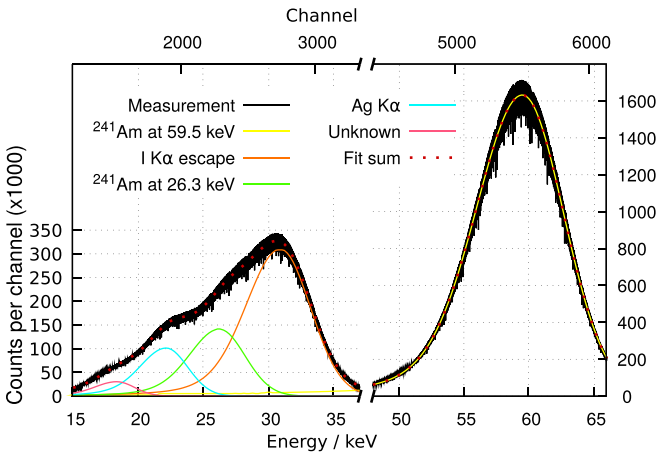

Fig. 7. The measured gamma spectrum with fitted Voigt profiles. The spectrum was cropped to show only the parts with a high enough number of counts. Note that the ordinate axis scales are different for the two peaks.

Table I. Gamma spectrum fit results. Peak energies and total number of counts are given for each peak seen in the measured gamma spectrum.

	Measured energy (keV)	Referent energy (keV) (Ref. 18)	Number of counts ($\times 10^6$)
^{241}Am at 59.5 keV	(calib)	59.5	1424.5 ± 1.3
I Kα escape	(calib)	59.5-28.6=30.9	196.4 ± 1.8
^{241}Am at 26.3 keV	26.23 ± 0.14	26.3	77.5 ± 3.9
Ag Kα	22.14 ± 0.12	22.16	48.0 ± 2.5
Unknown	18.35 ± 0.19	18.86	12.3 ± 1.7
Total	—	—	1756.9

peaks, while the peak at 59.5 keV has its own parameters. All 16 (6 Voigt + 5 ν_n + 5 A_n) of the fitting parameters were free, fitting and calibration was done iteratively until the calibration peaks matched the reference energies.

The final envelope follows the experimental data well and the fitted peak energies are given in Table I. The three peaks were identified as ^{241}Am gamma at 26.3 keV, Ag Kα at 22.16 keV (expected due to the source being internally wrapped in silver foil), and an unknown peak that lies in a severely attenuated part of the spectrum (possibly shifting the obtained energy).

Table I also contains the number of counts per peak, which can be used to calculate the probabilities. The ^{241}Am gamma at 59.5 keV is responsible for the I Kα escape peak and together they amount to a total of $(1620.9 \pm 2.2) \times 10^6$ events. The Ag Kα and the unknown peak may be excited by photons from either of the two ^{241}Am lines. Accounting this into the error, the probability ratio for the two ^{241}Am lines was determined to be (93.9 ± 1.7)% to (6.1 ± 1.7)%, which is in good agreement with the expected ratio of 94.05% to 5.95% following from data in Fig. 1.

C. Correlation heatmap

With the configuration used for our measurement, the acquired alpha and gamma spectra have a total of 2201 and 7992 channels, respectively. The observed coincidence interval was 20 μs, which with a sampling time of 8 ns amounts to 2500 steps. Since the counts are recorded in 32-bit unsigned integers, the resulting 3D array would be massive and steps of 25 channels had to be used for both spectra, giving a final array of 89 × 329 × 2500 elements. For the correlation diagram shown in Fig. 8, the number of correlated counts is calculated by subtracting the background from the correlated peak in the coincidence delay graph for each pixel representing 25 × 25 channels. The background is determined by counting all events in the first and last quarter of the coincidence delay graph for that pixel (as an example, the coincidence delay graph summed over all channels is shown in Fig. 9), assuming that the peak is completely situated within the central two quarters, which is achieved by a long enough coincidence window. The full alpha and gamma spectra also shown in the figure are aligned with the heatmap and as such indicate the correlated peaks.

In this case, there is apparently only one clearly visible peak in the alpha spectrum. However, when a correlation ratio heatmap (Fig. 10) is plotted where the pixels represent the correlated to background event ratio the alphas of higher energies seem to be more correlated with the gammas than those of lower energies, indicating that there might be more

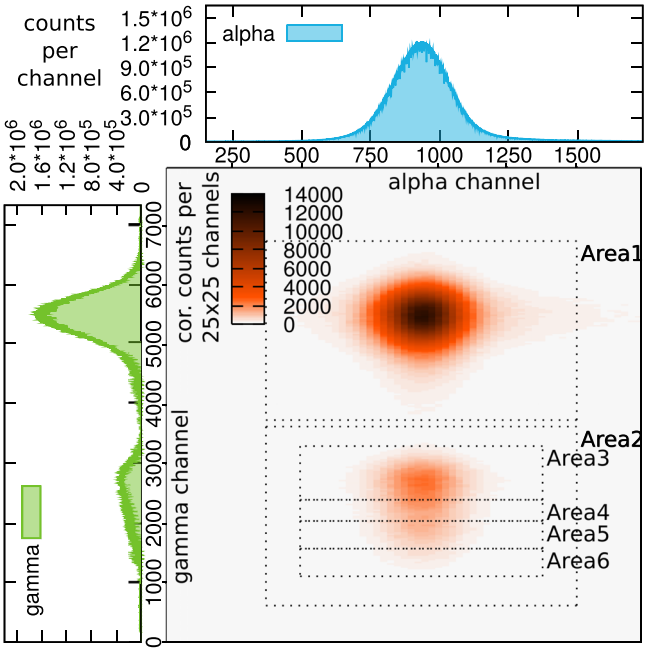

Fig. 8. The correlation heatmap. Each pixel represents the number of correlated counts (without the background) per 25 × 25α/γ channels.

than one alpha peak in the spectrum. The correlated to background event ratio is defined as

$$R_{mn} = \left[\frac{N_{\text{tot}} - N_{\text{bgnd}}}{N_{\text{bgnd}}}\right]_{mn}.$$

Here, N_{tot} is the total number of counts for the energy channels represented by the (m, n)th pixel, and N_{bgnd} is the background number of events for the same pixel, determined in the way described above. A cutoff value for the minimum number of events per pixel has to be introduced, otherwise the ratio of two background noise values widens the count heatmap range making the graph illegible. It can be seen that the ratio is not uniform across the peaks. The white pixels represent pixels with an insufficient number of counts for calculating the ratio.

The areas marked in Fig. 8 correspond to the total two peaks (Area1 and Area2) and the individual sub-peaks of the lower energy peak (Area3 through Area6) with their gamma boundaries corresponding to boundaries of equal level (i.e., curve crossings) shown in the gamma spectrum in Fig. 7. For

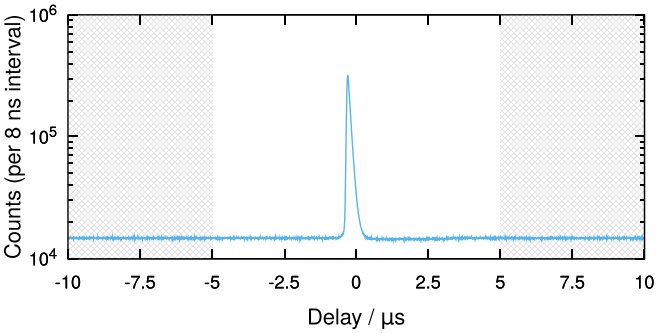

Fig. 9. Coincidence delay graph spanning the whole coincidence window including counts of all alpha and gamma channels. The hatched gray areas mark the parts used to determine the background.

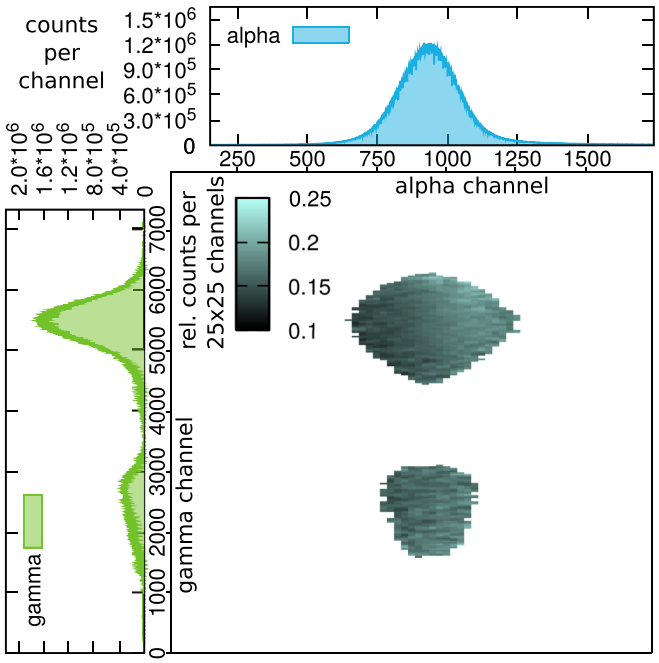

Fig. 10. The correlation ratio heatmap. Each pixel represents the ratio of the total correlated to total background number of counts per time interval.

each of the six areas, three files are exported. The first file is the coincidence delay graph which is integrated over all energies inside the area and is used in subsection III E for half-life calculations. The other two files are the alpha correlation spectrum (which is the number of counts per pixel integrated over all gamma energies in the area), and the equivalent gamma correlation spectrum, which are used in subsection III D.

D. Correlation spectra

The total alpha and correlated alpha spectra are shown in Fig. 6. Scaling the correlated spectrum revealed that it does not entirely match the total spectrum, but is in fact offset towards higher energies. This feature was also tested for each area marked in Fig. 8 with equal results. This finding implies there is another peak in the alpha spectrum, which is not correlated with any of the peaks in the gamma spectrum, and that all of the detected peaks in the gamma spectrum are correlated with the same peak in the alpha spectrum, which is consistent with theory. Fitting a Voigt with an asymmetric Lorentzian part first to the correlated spectrum, and then adding an additional peak and using only the amplitude from the first peak as a free parameter to fit their sum onto the total alpha spectrum yields the ratio of $(79 \pm 18)\%$ to $(21 \pm 18)\%$ for the correlated and uncorrelated peaks, both shown in Fig. 6. These values have high errors due to the large number (i.e., 5) of fit parameters, but are in agreement with the expected percentages shown in Fig. 1.

E. Half-lives

The coincidence delay graphs for each area are shown in Fig. 11 in logscale. The curves represent the number of gamma events occurring after an alpha event by the specified delay, while counting only events with energies within the corresponding area. With 8 ns timing resolution, it is possible to determine the half-life with good precision. Observing

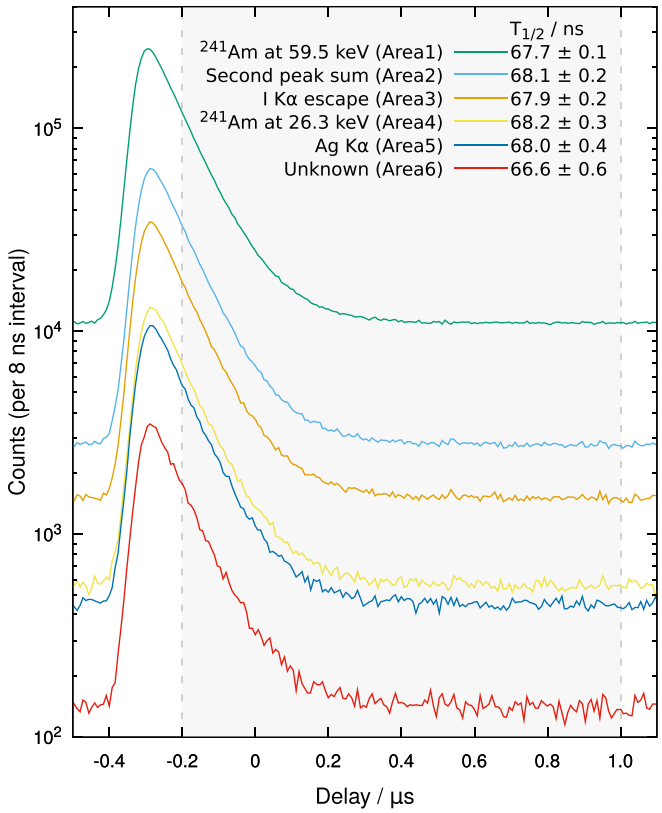

Fig. 11. Coincidence delay graphs with determined half-life values. The gray area marks the fit range used to determine half-lives.

the leftmost vertical dashed line, one may notice that the higher the gamma energy, the smaller the offset of the peak. This is an error due to the fact that the trigger level is non-zero, and the slope of the initial event signal depends on the peak height. However, this does not affect our results.

An exponential function of the form

$$N = N_0 + A \cdot 2^{-(t-t_0)/(\tau_{1/2})}$$

is fitted to each dataset, with boundaries shown by the gray area in Fig. 11. The fitting parameters are the noise constant N_0, the amplitude A, and the half-life $\tau_{1/2}$. The half-life of the ^{241}Am gamma at 59.5 keV was determined to be 67.7 ± 0.1 ns, which is compatible with the expected value of 67.2 ns. The half-lives of the other lines reside around 68.0 ± 0.5 ns, except for the last unknown line, which lies outside this interval. Here, we should note that Area3 through Area6 contain overlapping data, and as such the half-lives are mixed.

IV. CONCLUSIONS

We have set up a coincidence counting experiment using available university teaching equipment and an open-source DAQ platform. With custom software written for energy-resolved coincidence counting, we were able to sort the detected events by their alpha and gamma energies as well as delay between them. By fitting Voigt functions onto the total gamma spectra, we were able to determine the associated excited states. The obtained transition probabilities were a good match to the expected values. Visualizing the data in the form of a correlation heatmap allowed us to determine that all of the visible peaks in the gamma spectrum are

correlated with the same alpha peak, which is consistent with theory. Furthermore, a correlation ratio heatmap suggests the existence of at least one additional uncorrelated peak otherwise not visible in the alpha spectrum. With this technique, we show that binning counts by energy and visualizing the data using heatmaps can be used to extract additional information compared to a simple trigger system, and may possibly be applied to other measurements as well. Despite not being able to resolve more than one peak in the alpha spectrum, using the correlation data we were able to infer the existence of at least one additional uncorrelated peak in the alpha spectrum, and have determined that all of the visible peaks in the gamma spectrum are correlated with the same alpha peak, which is consistent with theory. The half-life of the state associated with the ^{241}Am gamma at 59.5 keV was determined to be 67.7 ± 0.1 ns, which is compatible with the expected value. The half-lives of the other lines were slightly higher, and since they correspond to the same state this difference could be due to other effects resulting from interaction with matter.

We have shown that it is possible to perform coincidence measurements with simple equipment and that these measurements provide results competitive with measurements done with dedicated research-grade hardware. To date, such experiments have been rarely performed at an undergraduate or graduate level because the required research-grade hardware is not readily available. With the low-cost setup we have described, such measurements are now accessible in the instructional lab and will provide students with invaluable insights into nuclear structure and decay schemes.

ACKNOWLEDGMENTS

The authors thank our technician Ljubomir Špirić, the laboratory technician at the Physics department in Rijeka for his assistance during the measurements. The authors also gratefully acknowledge valuable suggestions from the reviewers which considerably improved the article. This work was supported by the University of Rijeka grant "Improvement of teaching methods – development of measures for incorporating advanced e-learning tools in the curriculum."

[a]Author to whom correspondence should be addressed. Electronic mail: mkaruza@uniri.hr

[1]E. Sakai, H. Tamura, and Y. Sakurai, "Absolute measurements of the disintegration rates of americium-241 sources by using semiconductor detectors," J. Nucl. Sci. Technol. **1**(3), 101–109 (1964).
[2]A. A. Rollefson and R. M. Prior, "An advanced undergraduate nuclear lifetime experiment," Am. J. Phys. **46**(10), 1007–1008 (1978).
[3]M. Streun, G. Brandenburg, H. Larue, E. Zimmermann, K. Ziemons, and H. Halling, "Coincidence detection by digital processing of free-running sampled pulses," Nucl. Instrum. Methods Phys. Res. A **487**(3), 530–534 (2002).
[4]G. Suliman, S. Pommé, M. Marouli, R. Van Ammel, V. Jobbágy, J. Paepen, H. Stroh, C. Apostolidis, K. Abbas, and A. Morgenstern, "Measurements of the half-life of ^{214}Po and ^{218}Rn using digital electronics," Appl. Radiat. Isot. **70**(9), 1907–1912 (2012).
[5]J. Pechousek, R. Prochazka, V. Prochazka, and J. Frydrych, "Virtual instrumentation technique used in the nuclear digital signal processing system design: Energy and time measurement tests," Nucl. Instrum. Methods Phys. Res. A **637**(1), 200–205 (2011).
[6]G. Gamow, "Zur quantentheorie des atomkernes," Z. Phys. **51**, 204–212 (1928).
[7]B. R. Holstein, "Understanding alpha decay," Am. J. Phys. **64**(8), 1061–1071 (1996).
[8]D. Duarte and P. B. Siegel, "A potential model for alpha decay," Am. J. Phys. **78**(9), 949–953 (2010).
[9]P. M. Walker and G. D. Dracoulis, "Energy traps in atomic nuclei," Nature **399**, 35–40 (1999).
[10]David D. Clark, "Shape isomers and the double-humped barrier," Phys. Today **24**(12), 23–31 (1971).
[11]P. M. Walker and J. J. Carroll, "Ups and downs of nuclear isomers," Phys. Today **58**(6), 39–44 (2005).
[12]M. S. Basunia, Nuclear Data Sheets **107**, 2323–2422 (2006).
[13]Red Pitaya Web Site, <http://redpitaya.com/>.
[14]Red Pitaya OS, <https://github.com/RedPitaya/RedPitaya/>.
[15]AGC Github repository, <http://www.github.com/mvxe/agc/>. See file FPGA/rtl/ssla.v for the FPGA counter code.
[16]AGC processing Github repository, <http://www.github.com/mvxe/agc-proc/>.
[17]B. H. Armstrong, "Spectrum line profiles: The Voigt function," J. Quant. Spectrosc. Radiat. **7**(1), 61–88 (1967).
[18]Periodic Table and X-ray Energies, <https://www.bruker.com/fileadmin/user_upload/8-PDF-Docs/X-rayDiffraction_ElementalAnalysis/HH-XRF/Misc/Periodic_Table_and_X-ray_Energies.pdf>.